

ESTIMATION OF THE NEON/OXYGEN ABUNDANCE RATIO AT THE HELIOSPHERIC TERMINATION SHOCK AND IN THE LOCAL INTERSTELLAR MEDIUM FROM *IBEX* OBSERVATIONS

P. BOCHSLER^{1,8}, L. PETERSEN^{1,9}, E. MÖBIUS¹, N. A. SCHWADRON¹, P. WURZ², J. A. SCHEER², S. A. FUSELIER³,
D. J. MCCOMAS^{4,5}, M. BZOWSKI⁶, AND P. C. FRISCH⁷

¹ Space Science Center and Department of Physics, University of New Hampshire, 8 College Road, Durham, NH 03824, USA; bochsler@space.unibe.ch

² Physikalisches Institut, University of Bern, Sidlerstrasse 5, CH-3012 Bern, Switzerland

³ Lockheed Martin Advanced Technology Center, 3251 Hanover St., Palo Alto, CA 94304, USA

⁴ Southwest Research Institute, 6220 Culebra Rd., San Antonio, TX 78238, USA

⁵ Department of Physics and Astronomy, University of Texas, San Antonio, TX 78249, USA

⁶ Space Research Centre, Polish Academy of Sciences, Bartycka 18 A, PL 00-716 Warsaw, Poland

⁷ Department of Astronomy and Astrophysics, University of Chicago, 5640 S. Ellis Avenue, Chicago, IL 60637, USA

Received 2011 July 12; accepted 2011 September 19; published 2012 January 31

ABSTRACT

We report the first direct measurement of the Ne/O abundance ratio of the interstellar neutral gas flowing into the inner heliosphere. From the first year of *Interstellar Boundary Explorer IBEX* data collected in spring 2009, we derive the fluxes of interstellar neutral oxygen and neon. Using the flux ratio at the location of *IBEX* at 1 AU at the time of the observations, and using the ionization rates of neon and oxygen prevailing in the heliosphere during the period of solar minimum, we estimate the neon/oxygen ratios at the heliospheric termination shock and in the gas phase of the inflowing local interstellar medium. Our estimate is $(\text{Ne}/\text{O})_{\text{gas,ISM}} = 0.27 \pm 0.10$, which is—within the large given uncertainties—consistent with earlier measurements from pickup ions. Our value is larger than the solar abundance ratio, possibly indicating that a significant fraction of oxygen in the local interstellar medium is hidden in grains and/or ices.

Key words: ISM: abundances – ISM: atoms – Sun: heliosphere

1. INTRODUCTION

In the theory of nucleosynthesis neon and oxygen are classified as alpha-elements, i.e., nuclei whose most abundant isotopes consist of a multiple of helium nuclei. Oxygen and neon are mainly produced in massive stars with short lifetimes. Therefore, it is believed that the Milky Way has been rapidly enriched in these elements with the first few generations of stars. Their contemporary abundances in the interstellar medium (ISM) do not differ strongly from solar abundances, which reflect the composition of the ISM at the time of the formation of the Sun, 4.6 Gyr ago. Furthermore, since both elements are produced at similar sites and on similar timescales, one expects to find a ratio in the contemporary ISM close to the solar ratio.

Our study is motivated by the fact that because of the different ionization properties of oxygen and neon, the abundance ratio of these neutral species is spatially and temporarily strongly variable. It varies along the orbit of the Earth and also over the phases of solar activity. Mainly for the purpose of illustrating this variability in space and time, we have produced Figure 1. Adopting kinetic properties for neutral oxygen and neon in the local ISM inferred from those given by Witte (2004) for helium, we have carried out a Monte Carlo calculation to study the variability of the abundance ratio of neutral neon and oxygen along the Earth's orbit. In a first step we randomly injected particles from a distance 200 AU upstream of the Sun. The parameters describing the particle beams and the ionization properties are given in Table 1. In the second step, we calculated the survival probability of neutrals of those particles, which crossed the ecliptic plane at 1 AU. In the top panel of Figure 1 we show how the expected Ne/O ratio changes during times

of solar minimum. The Ne/O ratio is plotted in the ecliptic plane with angle zero pointing into the downwind direction (i.e., toward the gravitational focusing cone, where interstellar gas passing the Sun is focused owing to its gravitational attraction). The blue curve illustrates the variable Ne/O ratio; it is scaled to our measured value (see below) of 0.4 near 55° from the downwind direction. The ratio is lowest in the upwind direction, where it cannot be observed with the *Interstellar Boundary Explorer (IBEX)* owing to the configuration of *IBEX*'s spin axis, which is always pointing toward the Sun. At this point, the ratio reflects more closely its value at the heliopause because photoionization and ionization of oxygen by charge exchange with solar wind protons discriminate least between O and Ne. During periods of high solar activity, illustrated with the red curve in the bottom panel of Figure 1 with a different radial scale, oxygen is strongly suppressed, and practically only neon survives in the inner solar system down to 1 AU. Investigating the variability of this ratio under different conditions should reveal interesting details on heliospheric processes and is a prerequisite for interpreting kinetic properties (temperatures and higher moments of the velocity distributions) of oxygen and neon in the interface region.

Both elements have also been studied in the form of pickup ions in the inner heliosphere (Gloeckler & Geiss 2004; Drews et al. 2010). This is an additional reason for investigating the sources. Whereas oxygen undergoes charge exchange with protons in the heliopause, neutral neon travels practically unimpeded through the interface between heliosphere and ISM. This difference could lead to different observable kinetic properties of neutrals (and their respective pickup ions) near 1 AU. Investigating these properties adds motivation to disentangle the two species in the neutral flow through the inner heliosphere.

Reliable estimates of the contemporary interstellar Ne/O ratio have been inferred on a larger galactic scale from

⁸ Permanent address: Bahnhofstrasse 54, CH-3127 Mühlethurnen, Switzerland.

⁹ Now at University of Alaska, Fairbanks AK 99775, USA.

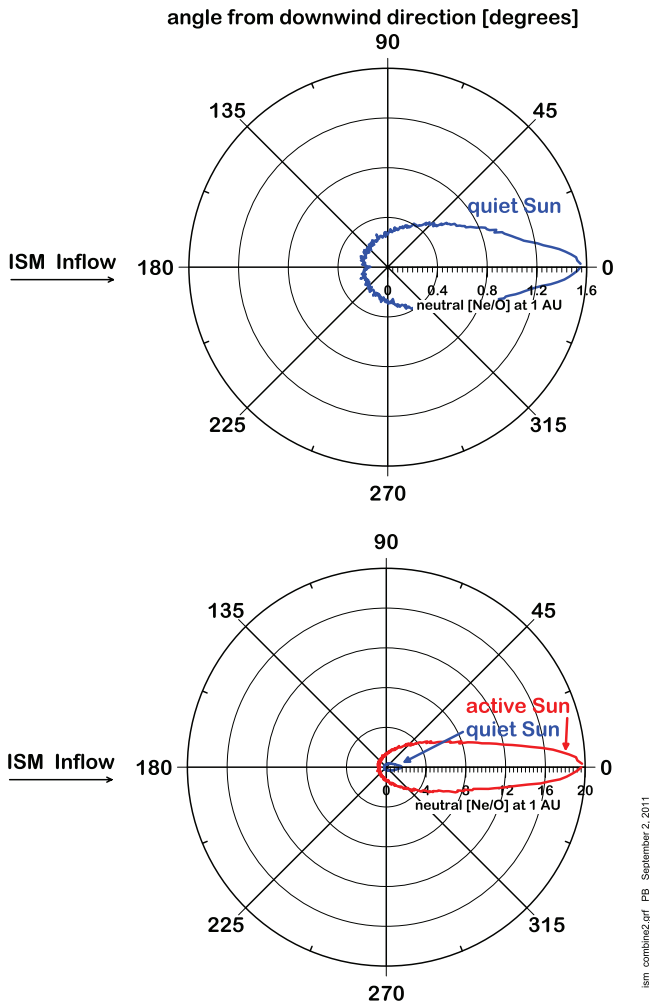


Figure 1. Abundance ratio of neutral interstellar neon and oxygen at 1 AU as a function of heliographic longitude. The figure shows the results of a Monte Carlo simulation with typical kinetic properties of these two interstellar species. Top panel: low solar activity; bottom panel, red curve: high solar activity (in the same scale for comparison: blue curve for low solar activity of the top panel). The results reported in this work correspond approximately to a location of *IBEX* near 125° from the direction of the instreaming interstellar gas.

X-ray spectroscopy of absorption edges in X-ray binaries by Juett et al. (2006). These authors find a Ne/O ratio of 0.185 ± 0.055 (including all ionization states), which is consistent with the solar value. On the other hand, Gloeckler & Fisk (2007) infer a ratio of 0.38 for the Ne/O ratio in the gas phase of the local ISM from pickup-ion data. Their value is significantly above the solar value. One therefore has to assume that a fraction of oxygen, comparable to the amount in the gas phase, is hidden in interstellar grains and ices to keep the total Ne/O abundance ratio in the local ISM consistent with its solar analog (Jenkins 2009). It should be noted, however, that the inference from heliospheric pickup ions for the local ISM rests strongly on the assumptions of their relative ionization state in the ISM and the respective filtration factors affecting their transition from the ISM into the heliosphere. Of course, the same problem applies for inferences from our measurements to the local ISM. Comparing different measurement strategies and inferences in the literature, one must be careful not to reason along circular arguments. We will address this problem in the discussion section of this paper. Hopefully, at some later stage of our investigation, the kinetic properties (temperature and higher moments of the velocity distributions) of secondary components

Table 1
Parameters Used for the Monte Carlo Simulation of Interstellar Neutral Oxygen and Neon Near 1 AU Shown in Figure 1

	Oxygen	Neon
Atomic mass (only one isotope considered)	16	20
Speed at infinity	26.3 km s^{-1a}	26.3 km s^{-1a}
Temperature at infinity	6300 K^a	6300 K^a
Ionization rate at 1 AU (active Sun)	$10.7 \times 10^{-7} \text{ s}^{-1}$	$6.5 \times 10^{-7} \text{ s}^{-1}$
Ionization rate at 1 AU (quiet Sun)	$4.1 \times 10^{-7} \text{ s}^{-1}$	$1.7 \times 10^{-7} \text{ s}^{-1}$

Note. ^a Witte (2004).

in the inflow of the ISM will provide some more details about relevant filtration processes.

On a technical level, this study provides the actual Ne/O ratio as observed by the *IBEX*-Lo sensor, which is a needed prerequisite for the determination of the temperature of heavy ISM constituents independent from the kinetic temperature of helium. These temperatures can directly be inferred from the observation of the angular distribution of the ISM flow at 1 AU, as discussed in the accompanying papers by Möbius et al. (2012) and Bzowski et al. (2012).

Concerning the comparison of the interstellar Ne/O with solar values, direct observations of neon in the solar photosphere are hampered by the fact that neon has the second highest first ionization potential of all elements and, correspondingly, high levels of excitation energy. Therefore, solar neon abundances have mainly been inferred from in situ measurements of solar particles. Both types of particles, solar energetic particles (SEPs) and the solar wind, yield consistent Ne/O abundance ratios of about 0.153 for SEPs (Reames 1998) and 0.14 for the solar wind (Bochsler 2007). Also the photospheric Ne/O ratio of 0.17 ± 0.05 derived from EUV observations with *Solar and Heliospheric Observatory*/Coronal Diagnostic Spectrometer is consistent with this value (Young 2005).

2. INSTRUMENTAL

The *IBEX* mission and the *IBEX*-Lo sensor have been described elsewhere (cf. McComas et al. 2009; Fuselier et al. 2009). The *IBEX*-Lo sensor is a single-pixel camera for energetic neutral atoms. The design of the entrance system is based on a cylindrical architecture with an annular collimator accepting neutrals in a field of view of $7^\circ \times 7^\circ$ in three 90° sectors and a 3.5×3.5 view angle in the fourth sector. Neutral particles that pass the collimator encounter a diamond-like conversion surface, which upon contact converts a small fraction of them into negative ions. The backscattering probability of incoming particles depends strongly on their energy, and the probability of a particle to undergo ionization depends strongly on its energy as well. After the conversion process, the ionized particles pass through a toroidal electrostatic energy per charge analyzer, which has been designed to accept a large angular range of backscattered and sputtered products from the conversion surface (Wieser et al. 2007). Finally, the negatively ionized particles are accelerated through a potential step of +16 kV and registered in an attached time-of-flight mass analyzer. The time-of-flight system uses triple coincidences to distinguish valid start and stop pulses from background pulses and thus suppresses background very efficiently. Of particular interest for the mass analysis is the fact that the system contains two subsequent paths, and three different times of flight can be measured independently from each other: the time of flight in the first path is denoted with “TOF1,” passage through the second path in sequence is

measured with “TOF2,” whereas the time for the total path is measured with TOF0. For our analysis only particles that fulfill the criterion $\text{TOF0} = \text{TOF2} + \text{TOF1}$ have been included (see Fuselier et al. 2009 for details on the electronic implementation of the checksum). Furthermore, since each registered particle has passed two ultrathin carbon foils at two slightly different energies, simultaneous measurements of TOF1 and TOF2 can be used to disentangle different sputter products such as C and O from the conversion surface almost unambiguously. However, for this first analysis in the following, only TOF2 has been used.

3. CALIBRATION

Testing and calibration of the *IBEX*-Lo sensor was carried out in several campaigns at the “MEFISTO” facility of the University of Bern (cf. Marti et al. 2001; Wieser & Wurz 2005). Using a neutral atom beam of different elements (H, He, C, O, Ne), which impact on the conversion surface, the detection efficiency of the *IBEX*-Lo sensor has been determined by measuring the amount of detected sputter products escaping from the conversion surface and the amount of converted, backscattered projectiles. For both types of products only negatively charged particles can be detected. For our purpose it is important to note that neon has no stable or metastable negative ion configuration and therefore cannot be identified as a converted ion; however, it is detectable through sputtered C and O, which are released from the conversion surface. Oxygen, on the other hand, is detectable as a negative ion when it is backscattered from the conversion surface, and it produces negatively charged sputter products as well. An extensive investigation of these various processes in the MEFISTO calibration facility led to the required knowledge of the branching ratios C/O for Ne and O and to the relative conversion efficiencies for both elements.

An example of two time-of-flight spectra produced during calibration is shown in Figure 2. Whereas the neon beam (top panel of Figure 2) produced almost equal amounts of C and O in the form of sputter products, backscattered oxygen dominated the registered particles in the time-of-flight system during irradiation with an oxygen beam, and comparatively little sputtered carbon was detected. The shape of the time-of-flight distributions in Figure 2 is typical for particles passing thin carbon foils: while electronic interactions within the solid lead to a more or less continuous deceleration of the projectiles and to some widening of their energy distributions, few close encounters with nuclei lead to deflection and strong energy loss and, correspondingly, to wide tails toward long times of flight, producing the skewed appearance of mass peaks as is evident in Figure 2.

We used an exponentially modified Gaussian $C(t)$, which is essentially a convolution of an exponential with a normal distribution, to fit the observed peaks (e.g., Li & McGuffin 2008, or Golubev 2010 for a more elaborate discussion). The Gaussian part, $G(t)$, of the distribution can be visualized as the result of a broadened initial energy distribution of sputtered and post-accelerated particles due to the electronic stopping within the carbon foil(s), whereas the exponential part, $E(t)$, convoluted with the Gaussian, is a consequence of the nuclear stopping within the carbon foil(s)

$$G(t) = \frac{1}{a_2\sqrt{2\pi}} \exp\left(-\frac{(a_1 - t)^2}{2a_2^2}\right), \quad (1)$$

$$E(t) = \frac{\exp\left(-\frac{t}{a_3}\right)}{a_3}, \quad (2)$$

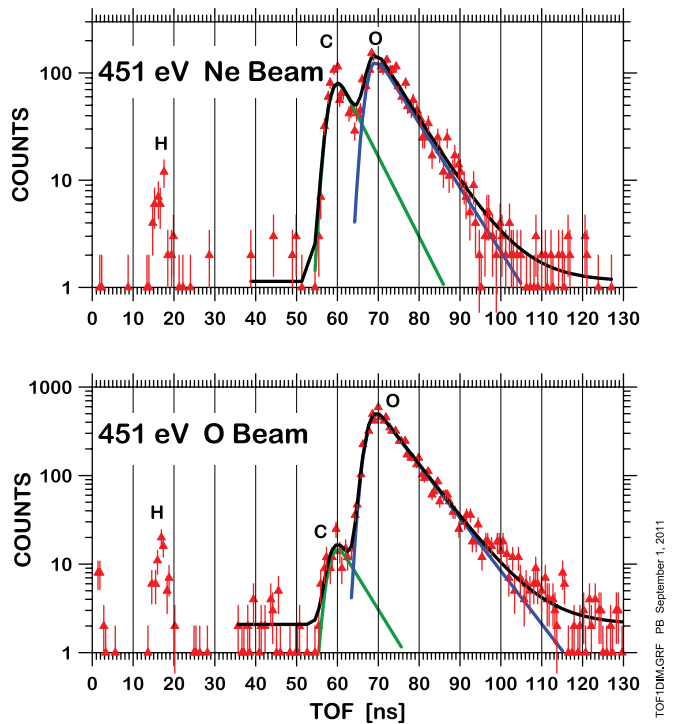


Figure 2. Distribution of times of flight as registered with the *IBEX*-Lo sensor during calibration at the MEFISTO facility of the University of Bern. These calibrations were carried out with a neutral neon beam (top panel) and an oxygen beam (bottom panel) at energies of interstellar neutrals at 1 AU and an instrument setting capable of detecting both backscattered and sputtered particles from the conversion surface. The data points (red triangles) have been fitted for both panels simultaneously using the maximum-likelihood technique with an 11-parameter fit using exponentially modified Gaussians (see the text). The blue line shows the fitted contribution of the backscattered and sputtered oxygen ions, while the green line represents the contribution of sputtered carbon ions. The black line is a superposition of carbon, oxygen, and background counts.

leading to

$$C(t) = \frac{a_0}{2a_3} \exp\left(\frac{a_2^2}{2a_3^2} + \frac{a_1 - t}{a_3}\right) \left[\operatorname{erf}\left(\frac{t - a_1}{\sqrt{2}a_2} - \frac{a_2}{\sqrt{2}a_3}\right) + 1 \right], \quad (3)$$

where $C(t)$ denotes the number of counts per time-of-flight bin. The parameter a_0 is a measure of the area under the peak, a_1 is the peak position, a_2 is the width of the Gaussian, and a_3 characterizes the decay of the exponential distribution.

4. FLIGHT DATA ANALYSIS

The data points shown as triangles in Figure 2 have been fitted using the maximum-likelihood technique for both panels simultaneously with basically the same minimal set of physical parameters as outlined in the previous section. In addition to the parameters for the exponentially modified Gaussian distribution, two free parameters have been used to describe constant background count rates for each panel. The decay times of the exponential distributions for sputtered carbon and oxygen have been linked by a predetermined scaling factor obtained from Stopping and Range of Ions in Matter program package simulations. Similarly, the peak locations have been fixed to the same values for the two calibration runs shown in the two panels. One notices a slightly faster decay of the carbon distribution (full green lines) compared to the oxygen tails (blue lines). The full black line is the superposition of the distributions including the background.

In principle, *IBEX*-Lo uses eight different energy passbands defined by the setting of the electrostatic E/Q analyzer. However, in order to accommodate a wide range of sputtered particles without strongly discriminating between O and C, we only considered one wide energy passband centered at an energy well below the expected energy of incoming particles corresponding to approximately 200 eV/e.

For the evaluation of our flight results we need three ingredients from the calibration data: (1) the ratio of the carbon-to-oxygen yield, observed with a pure neon beam, denoted with the symbol α ; (2) the ratio of the carbon-to-oxygen yield, found with a pure oxygen beam, denoted with β ; and (3) the ratio of the oxygen detection efficiencies for a neon and an oxygen beam, respectively, which is denoted with γ .

Then using the letter x for the C/O ratio measured in flight with *IBEX*, we are able to derive the flux-ratio Ne/O of interstellar neutrals at the location of observation with the above quantities

$$\frac{\Phi(\text{Ne})}{\Phi(\text{O})} = \frac{\beta - x}{\gamma \cdot (x - \alpha)}. \quad (4)$$

A detailed error analysis shows that from the calibration parameters, the parameter γ , i.e., the ratio of detection efficiencies of neon and oxygen, has the strongest influence on the final result. Unfortunately, to this moment, this value could only be determined from our calibration runs with a rather large uncertainty of approximately 30%. The values used for this evaluation and their corresponding uncertainties, mainly caused by limited reproducibility during the calibration procedure, are $\alpha = 1.28 \pm 0.082$, $\beta = 0.0489 \pm 0.0032$, $\gamma = 0.40 \pm 0.14$. From the flight data we derived a C/O ratio of $x = 0.217 \pm 0.024$. This leads to a neutral element flux ratio at 1 AU and at a heliographic longitude of about 125° from the upwind direction

$$\frac{\Phi(\text{Ne})}{\Phi(\text{O})} = 0.40 \pm 0.15. \quad (5)$$

For the following discussion, we will not distinguish between flux ratios, density ratios, and abundance ratios, as we expect neutral neon and oxygen to enter and travel through the heliosphere with the same speed.

5. RESULTS

As outlined in the introduction, the above value $\Phi(\text{Ne})/\Phi(\text{O})$ changes strongly over space and time. To a good approximation ionization by charge exchange with solar wind ions and photoionization vary with the inverse square of the heliocentric distance. This greatly simplifies inferences for the abundance ratio of neutral neon/oxygen at the location of the heliospheric termination shock.

The loss rate of neutrals approaching the Sun obeys a simple radial dependence

$$dN = -N(r) \frac{v_{(\text{ion},E)} \cdot r_o^2 \cdot dt}{r^2}. \quad (6)$$

Here, $N(r)$ is the neutral particle density (per m^3) at heliocentric distance r , $v_{(\text{ion},E)}$ denotes the loss rate of neutrals due to ionization at the reference distance, 1 AU, and r_o is the reference distance of 1 AU. This differential equation is easily solved considering Kepler's second law

$$h = r^2 \frac{d\theta}{dt} = \text{const.} \quad (7)$$

Substituting r^2 in Equation (6) with the relation for the angular momentum h of the particle yields

$$dN = -N \cdot \frac{v_{(\text{ion},E)} \cdot r_o^2 \cdot d\theta}{h}. \quad (8)$$

The only remaining independent variable is the true anomaly of the particle, θ , and Equation (8) can be integrated with the initial condition $N(\theta_\infty) = N_\infty$. Given the true anomaly of an incoming neutral particle at the site of observation, θ , and the true anomaly of the same particle in the upwind direction, θ_∞ , the surviving fraction of neutrals at the point of observation related to their amount at infinity is

$$\frac{N(\theta)}{N_\infty} = \exp \left[-\frac{v_{(\text{ion},E)} \cdot r_o \cdot (\theta - \theta_\infty)}{V_{(\text{neutral},1\text{AU})}} \right]. \quad (9)$$

In this last expression, the angular momentum of the particle, h , has been replaced by the angular momentum at perihelion, $V_{(\text{neutral},1\text{AU})} \cdot r_o$. The perihelion is incidentally the site of observation, because *IBEX*—owing to its particular viewing direction perpendicular to the solar direction—always observes particles near their perihelion, no matter where *IBEX* is located (Lee et al. 2012).

$V_{(\text{neutral},1\text{AU})}$ denotes the speed of a neutral particle at 1 AU, which has entered the solar system with a typical speed of ISM neutral helium of 22.8 km s^{-1} (Bzowski et al. 2012). We adopt ionization rates at 1 AU typical for the solar minimum, i.e., $4.09 \times 10^{-7} \text{ s}^{-1}$ for oxygen and $1.75 \times 10^{-7} \text{ s}^{-1}$ for neon (P. Bochsler et al. 2012, in preparation). For our location of observation, we insert $\theta - \theta_\infty = 125^\circ$, leading to surviving fractions of 6.2% of neutral oxygen and of 30.3% for neutral neon. Our measurement of this ratio at 1 AU yielded 0.40 ± 0.15 ; consequently, we infer a ratio of neutrals at the termination shock of $(\text{Ne}/\text{O})_{\text{neutral,TS}} = 0.081 \pm 0.030$.

6. DISCUSSION AND CONCLUSIONS

In the previous section we extrapolated the neutral Ne/O abundance ratio at the termination shock (TS) from the neutral Ne/O ratio observed at 1 AU, considering the ionization processes inside the heliosphere. The next step, to infer the total Ne/O abundance ratio in the unperturbed local ISM from the neutral Ne/O ratio at the termination shock, requires correction for ionization in the interface between the heliosphere and the ISM and in the ISM itself. Filtration factors are defined as the ratio of the neutral density of a species just inside the solar wind termination shock to its neutral density in the unperturbed ISM (Cummings et al. 2002).

For the further discussion we use Figure 3, which is a schematic one-dimensional representation of abundances of neon and oxygen in the heliosphere, the surrounding local ISM, and the interface between the two regions. Ionization levels of oxygen and hydrogen are tightly coupled by forward and reverse charge exchange ($\text{H}^+ + \text{O} \leftrightarrow \text{O}^+ + \text{H}$), so that the density of neutral interstellar oxygen is amplified above the interstellar value by a factor of up to 1.9 in the outer heliosheath (Müller & Zank 2004). In the numerous different heliospheric models in Müller & Zank (2004) and Izmodenov et al. (2004), the total oxygen filtration between the ISM and TS ranges from 0.7 to 1.3, where values larger than 1 indicate the augmentation of interstellar densities. The 50% uncertainty of the oxygen filtration values adds to a similar uncertainty in the estimated neutral Ne/O ratio, which further propagates onto the total

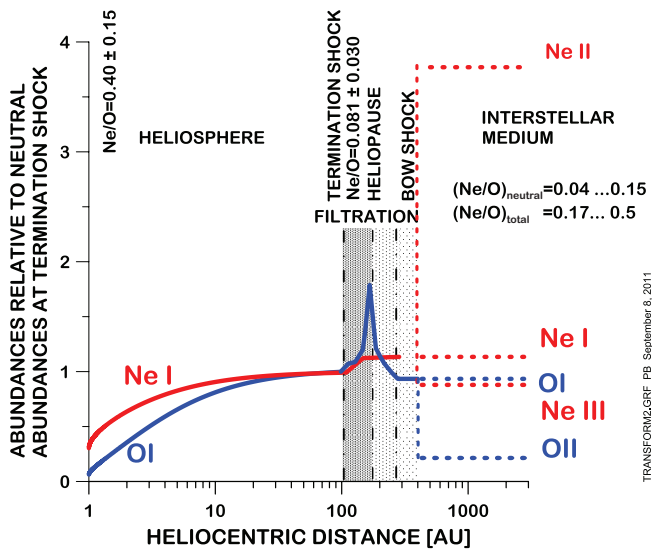


Figure 3. Schematics of transfer of neon and oxygen through the interface between the local interstellar medium and the heliosphere. Only neutral species can penetrate into the inner heliosphere. In order to estimate the total neon/oxygen abundance ratio in the ISM from neutrals inside the heliosphere, one needs to know the ionization state of these elements in the ISM. The relative abundances of the various charge states of neon and oxygen in the ISM were taken from Model 26 of Slavin & Frisch (2008). The filtration factors indicating the losses of neutral neon through photoionization on the way from the bow shock through the heliopause to the termination shock were adopted from Cummings et al. (2002). The profile of model A of Müller & Zank (2004) is used to illustrate the oxygen wall near the heliopause. The further decrease of neutral neon and oxygen during the travel to 1 AU was computed for conditions near solar minimum. The abundances of neutral neon and oxygen were normalized to 1 at the termination shock.

Ne/O abundance ratio in the ISM. The abundances of oxygen and neon have been normalized to 1 at the termination shock in Figure 3. The location and structure of the interface have been adapted from Müller & Zank (2004). Inside the termination shock full curves show the decrease of neutral neon (red) and neutral oxygen (blue) due to the effect of ionization as the gas approaches the Sun.

Adopting the filtration factors given by Izmodenov et al. (1999) for oxygen of 0.70 and by Cummings et al. (2002) for neon of 0.88, we derive from our estimation of the neutral ratio $(\text{Ne}/\text{O})_{\text{neutral,TS}} = 0.081 \pm 0.030$ at the termination shock, and for the neutral density ratio in the local ISM a value of $(\text{Ne}/\text{O})_{\text{neutral,ISM}} = 0.064 \pm 0.025$. The published uncertainties of these filtration factors have almost no influence on the overall uncertainty of this ratio, given the large uncertainty of our estimate of the neutral abundance ratio at 1 AU.

Nevertheless, several caveats are appropriate: the model of Cummings et al. (2002), which was essentially intended to describe the impact of filtration on anomalous cosmic rays, is one-dimensional. It is clear that different assumptions on parameters for numerical simulations of the interface between the ISM and the heliosphere change the adopted filtration factors. The wide range of O filtration factors predicted by different simulations, from 0.7 to 1.3, including the uncertainties of the value derived inside the termination shock, yields a neutral interstellar Ne/O abundance ratio in the range of 0.04–0.15. Furthermore, one has to keep in mind that the filtration factors based on the models of Izmodenov et al. (1999) and Müller & Zank (2004) might undergo some changes, since these models need revision incorporating the new value for the velocity of the interstellar gas at infinity, derived from *IBEX* measurements by Möbius et al. (2012) and Bzowski et al. (2012).

Finally, in order to compare the total abundance ratio of neon over oxygen in the local ISM, one has to consider that only fractions of O and Ne are present in neutral form at the outer interface. Using the ionization fractions of Model 26 of Slavin & Frisch (2008) to be 0.804 for neon and 0.186 for oxygen, and using our extrapolated value of $(\text{Ne}/\text{O})_{\text{neutral,ISM}} = 0.064 \pm 0.025$ and restricting the filtration factors to 0.7 for O and 0.88 for Ne, we have to conclude that the Ne/O gas+ion density ratio is $(\text{Ne}/\text{O})_{\text{gas,ISM}} = 0.27 \pm 0.10$, which is larger than the solar ratio. It is also larger than the overall ratio published by Juett et al. (2006). A filtration factor of 1.3 for oxygen, as proposed by Müller & Zank (2004), would yield a ratio as high as $(\text{Ne}/\text{O})_{\text{gas,ISM}} = 0.5$. While it seems beyond doubt that all available neon species in the ISM in gaseous and ionic form are included in such balance considerations, it is possible that oxygen is also present in solids in the local ISM. A deficit of oxygen in gaseous form as is indicated by the discrepancy between the interstellar and the solar neon/oxygen ratio requires that some oxygen is hidden in the form of grains and/or ices. Jenkins (2009) has thoroughly investigated the gas-phase depletion of many elements in the ISM and come to the surprising conclusion that oxygen seems even more depleted than rather refractory elements such as Mg, Si, and Fe. One possibility is that large amounts of oxygen are buried in thick layers of water ice on large dust grains and become even undetectable by X-rays. However, it is questionable that such a scenario could be relevant for the relatively tenuous ISM in the close vicinity of the heliosphere.

We thank all the individuals who have contributed to the success of the *IBEX* mission. This work was supported by the *Interstellar Boundary Explorer* mission as a part of NASA's Explorer Program, in particular SR&T Grant NNX09AW32G and contract NNG05EC85C for the *IBEX* mission, and by the Swiss National Science Foundation. We also acknowledge grant N-N203-513-038 from the Polish Ministry for Science and Higher Education. We thank an anonymous referee for constructive comments.

REFERENCES

- Bochsler, P. 2007, *A&A*, 471, 315
 Bzowski, M., Kubiak, M. A., Möbius, E., et al. 2012, *ApJS*, 198, 12
 Cummings, A. C., Stone, E. C., & Steenberg, C. D. 2002, *ApJ*, 578, 194
 Drews, C., Berger, L., Wimmer-Schweingruber, R. F., et al. 2010, *J. Geophys. Res.*, 115, A10108
 Fuselier, S. A., Bochsler, P., Chornay, D., et al. 2009, *Space Sci. Rev.*, 146, 117
 Gloeckler, G., & Fisk, L. A. 2007, *Space Sci. Rev.*, 130, 489
 Gloeckler, G., & Geiss, J. 2004, *Adv. Space Res.*, 34, 53
 Golubev, A. 2010, *J. Theor. Biol.*, 262, 257
 Izmodenov, V. V., Lallement, R., & Geiss, J. 1999, *A&A*, 344, 317
 Izmodenov, V. V., Malama, Y. G., Gloeckler, G., & Geiss, J. 2004, *A&A*, 414, L29
 Jenkins, E. B. 2009, *ApJ*, 700, 1299
 Juett, A. M., Schulz, N. S., Chakrabarty, D., & Gorzyca, T. W. 2006, *ApJ*, 648, 1066
 Lee, M. A., Kucharek, H., Möbius, E., et al. 2012, *ApJS*, 198, 10
 Li, X., & McGuffin, V. L. 2008, *J. Chromatogr. A*, 1203, 67
 Marti, A., Schletti, R., Wurz, P., & Bochsler, P. 2001, *Rev. Sci. Instr.*, 72, 1354
 McComas, D. J., Allegrini, F., Bochsler, P., et al. 2009, *Space Sci. Rev.*, 146, 11
 Möbius, E., Bochsler, P., Heirtzler, D., et al. 2012, *ApJS*, 198, 11
 Müller, H.-R., & Zank, G. 2004, *J. Geophys. Res.*, 109, A07104
 Reames, D. V. 1998, *Space Sci. Rev.*, 85, 327
 Slavin, J. D., & Frisch, P. C. 2008, *A&A*, 491, 53
 Wieser, M., & Wurz, P. 2005, *Meas. Sci. Technol.*, 16, 2511
 Wieser, M., Wurz, P., Möbius, E., et al. 2007, *Rev. Sci. Instr.*, 78, 124502
 Witte, M. 2004, *A&A*, 426, 835
 Young, P. R. 2005, *A&A*, 444, L45